Progress In Electromagnetics Research Letters, Vol. 94, 35–41, 2020

A Novel Frequency Selective Surface with Two Non-Interfering Passbands

Chenglong Wang[1, 2] and Chunyang Wang[1, 3, *]

Abstract—A novel dual-band frequency selective surface (FSS) operating at Ku- and Ka-bands is presented in this paper. The proposed FSS is an aperture element constituted by a square loop loaded with four symmetrical umbrella-shaped stubs on the front side of the dielectric substrate. A good angular stability up to 60° angle of incidence for both TE and TM polarizations is provided by the FSS. Moreover, the two passbands of FSS can be controlled independently and flexibly by changing corresponding structural parameters. A prototype of the FSS is fabricated and measured. The good agreement between simulation and measurement results further proves the performance of the FSS.

1. INTRODUCTION

Working as a spatial filter, traditional frequency selective surface (FSS) is constituted by an infinite array of metallic patterns printed on a dielectric substrate to control the transmission and reflection of an incident electromagnetic wave [1]. Additionally, it is reported that FSSs can be made of different materials, like all-dielectric materials [2], printed surfaces [3], or all metal structures [4]. Since natural materials do not possess the characteristic of frequency selectivity, FSS is also classified as the concept of metasurface by some scholars, which has gained a lot of attention over the past decade [5–10]. In fact, the time that FSS was proposed is much earlier than that of metasurface. Now FSSs have extensive application in microwave and millimeter-wave regimes, such as radomes, antennas, and absorbers [11–15]. With the rapid development of multi-functional wireless communication devices, FSSs with multiple independent transmission bands are especially demanded.

Up to now, a lot of techniques and approaches to design multiband FSSs are reported in the literature. As a new trend of FSS design, artificial intelligence-based approaches, such as Particle Swarm Intelligence, have been used to design FSSs [16–18]. In article [19], a dual-band FSS composed of a closed loop and its complementary structure is presented first. Then, Zanganeh et al. proposed an FSS structure, which can obtain dual-band characteristics by using non-resonant units [20]. Moreover, some dual-band FSSs based on cascading technology are also given in [21–24]. Although this method is easy to achieve multiband FSSs, their thicknesses are usually too large. Adopting various resonant elements or fractal elements is another common way to realize single-layered multiband FSSs [25–28]. However, the higher order mode of multiband FSSs is not stable especially for large angle incidence and large frequency ratio (ratio of higher resonant frequency to lower resonant frequency). Recently, a novel three dimensional (3D) dual-band FSS with better performance and flexibility than traditional dual-band FSS is reported [29]. It also has some deficiencies, such as larger insertion loss, higher profile than traditional dual-band FSS and great difficulty in fabrication. Considering the previous research

Received 17 June 2020, Accepted 11 September 2020, Scheduled 20 October 2020

* Corresponding author: Chunyang Wang (cywangcl@163.com).

[1] Changchun University of Science and Technology, Changchun 130033, China. [2] Changchun Institute of Optics, Fine Mechanics and Physics, Chinese Academy of Sciences, Changchun 130033, China. [3] Northwest Institutes of Advanced Technology, Xi'an Technological University, Xi'an 710000, China.

on dual-band FSSs, a single-screen FSS with stable dual-band filtering characteristics and independent controllability is rarely mentioned.

In this paper, a single-layered FSS operating at Ku- and Ka-bands with center frequency of 16.6 GHz and 37 GHz is proposed. The novel designed FSS exhibits a good resonance stability under various incident angles for both TE and TM polarizations due to the miniaturized element with a size of $0.133\lambda_0 \times 0.133\lambda_0$. Furthermore, by changing the corresponding structural parameters of FSS elements, the two passbands of proposed FSS can be controlled independently and flexibly. The measurement results of an FSS prototype well coincide with numerical simulations, verifying the validity of our design.

2. MODEL AND ANALYSES

Figure 1 depicts the unit cell geometry of the proposed FSS. The FSS consists of a square loop loaded with four symmetrical umbrella-shaped stubs on the front side of the dielectric substrate, where the gray areas denote metallic structures, while the other areas represent slots. Such a novel design can effectively decrease the resonant frequency, which further results in lower sensitivity to incident angles. Commercially available polyimide with $\varepsilon_r = 3$ and $\tan\delta = 0.005$ has been used as a dielectric substrate. The dimensions of the unit cell are: $p_x = p_y = 2.4\,\text{mm}$, $g_1 = 0.16\,\text{mm}$, $g_2 = 0.1\,\text{mm}$, $g_3 = 0.1\,\text{mm}$, $w = 0.1\,\text{mm}$, $l_1 = 0.72\,\text{mm}$, $l_2 = 0.53\,\text{mm}$, $l_3 = 0.88\,\text{mm}$, and $t = 0.0254\,\text{mm}$.

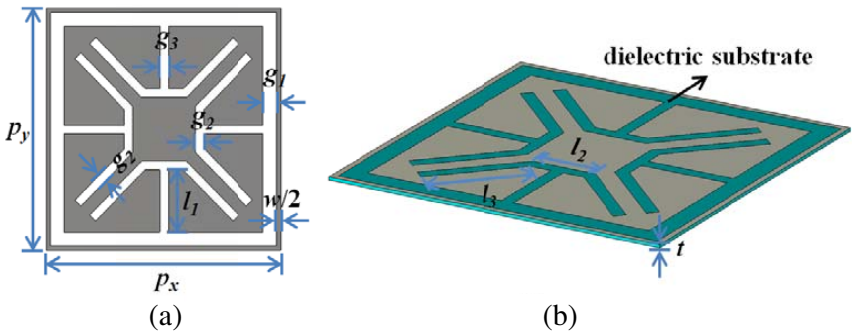

Figure 1. Sketch of the proposed FSS: (a) front view; (b) side view.

The design process of the FSS element is illustrated in Figure 2. The origin of the structure is an aperture element consisting of four symmetrical split-ring resonators (SRRs) combined with a square loop element. Next, the four SRRs move inward together, thus forming the final pattern. It should be noted that the SRRs are arranged symmetrically in order to ensure the polarization stability of unit cell. According to the design process, the lower and higher resonant frequencies can be controlled by changing the areas of square loop and SRRs, which are respectively denoted by red and blue arrow lines in Figure 2. Physically, the perimeter of the square loop is close to a wavelength of the lower resonant frequency, while the length of the SRR is approximate to a half-wavelength of the higher resonant frequency.

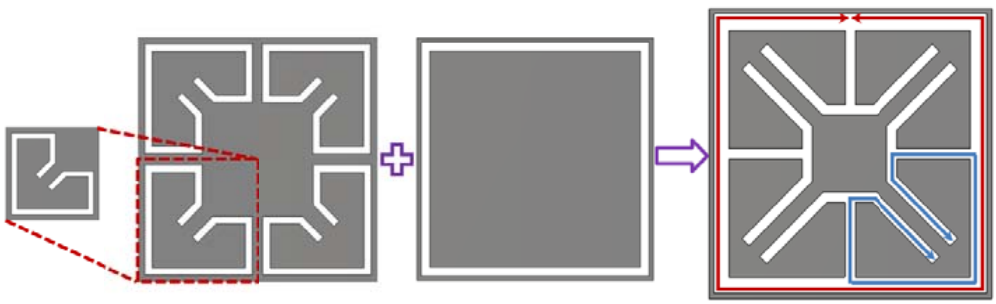

Figure 2. Design process of the proposed FSS element.

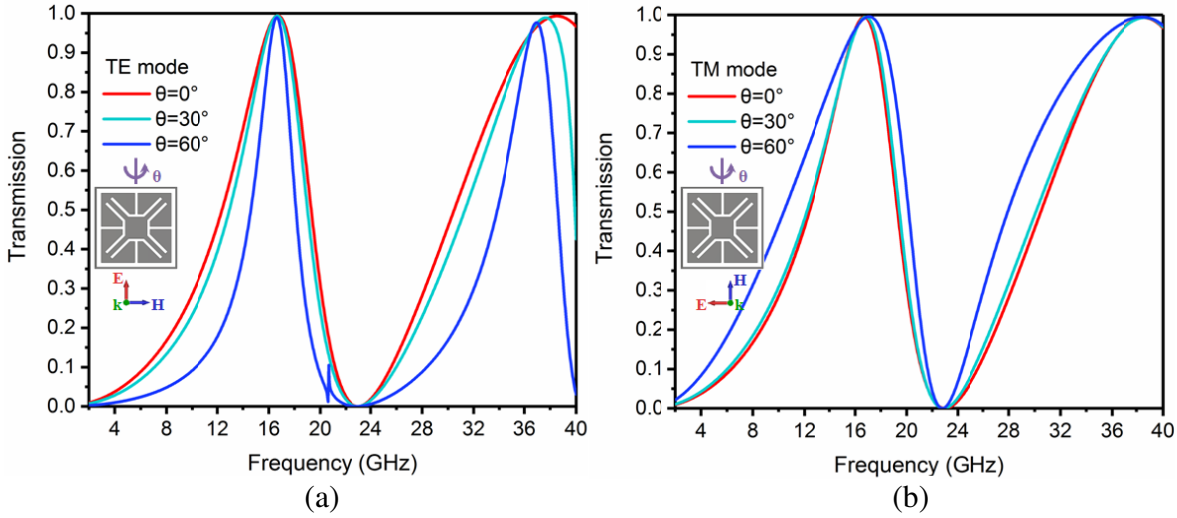

Figure 3. Simulated transmission of the proposed FSS under various incident angles: (a) TE polarization; (b) TM polarization.

To validate the aforementioned performance, a full-wave simulation of the proposed FSS is executed in the commercial software CST. In this simulation, the boundary conditions of unit cell were used to mimic infinite FSS structure, and two Floquet ports were set as the excitation source. The transmission coefficients were expressed in terms of an S-matrix, and they could be calculated directly from the inputs related to Floquet modes with various incident angles. The simulated transmission of the proposed FSS under various incident angles for both TE and TM polarizations is shown in Figure 3. It is observed from Figure 3 that the proposed FSS can provide two passbands resonating at 16.6 GHz and 37 GHz for TE and TM polarizations, respectively. Moreover, both the resonances are stable up to 60° angle of incidence, while the frequency shift of two passbands is less than 4%. Obviously, the good resonance stability of FSS with respect to different incident angles and polarizations is verified, which is attributed to the miniaturized unit cell with the size of $0.133\lambda_0 \times 0.133\lambda_0$ (λ_0 is the free-space wavelength of the lower resonant frequency).

Besides the good resonance stability mentioned above, the designed FSS also possesses great flexibility to independently control the frequencies of two passbands just by adjusting structural parameters. In the procedures of numerical simulation, the law that the lower resonant frequency mainly relates to area of square loop and the higher resonant frequency chiefly depends on area of umbrella-shaped stubs was discovered. Figure 4 further describes the simulated transmission of the proposed FSS with respect to structural parameters under normal incidence.

As illustrated in Figure 4(a), the larger the width g_1 of the square loop is, the higher the first resonant frequency is, while the second resonant frequency remains almost constant. Figure 4(b) shows that the second resonant frequency shifts to higher frequency while the first resonant frequency is nearly unchanged, as the width g_2 of the umbrella-shaped stubs increases and the length l_3 of the arm of stubs decreases properly and simultaneously. The independent control of two passbands means that different operation bands can be achieved easily.

In order to explain the physical mechanism of the proposed FSS, the electric field distributions of the structure at two passband frequencies for TE polarization under normal incidence are given in Figure 5. As shown in Figure 5(a), the electric field is mostly distributed in the square loop and the rods of umbrella-shaped stubs along the horizontal direction at 16.6 GHz for TE polarization under normal incidence. This kind of field distribution signifies that the resonance at lower frequency of FSS is chiefly determined by the areas of square loop and rods. In contrast, from the Figure 5(b), we can discover that the electric field mainly focuses on the horizontal umbrella-shaped stubs at 37 GHz for TE polarized wave with incident angle of 0 degrees, which can indicate that the area of stubs primarily contributes to the resonance at higher frequency.

In general, to ensure that the four umbrella-shaped stubs are compact, the length of rods would

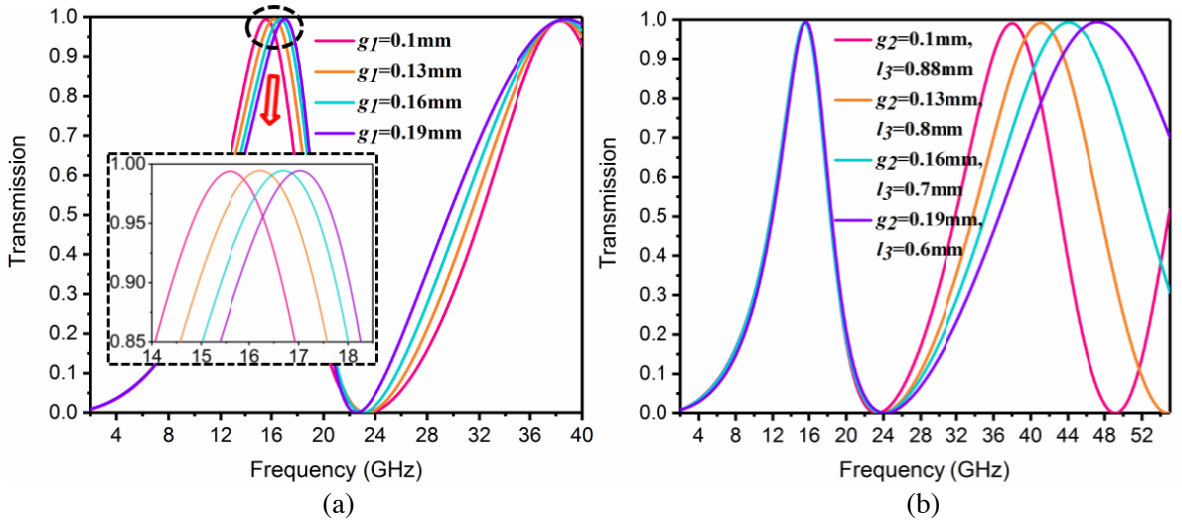

Figure 4. Simulated transmission of the proposed FSS under normal incidence as a (a) function of g_1 and (b) function of g_2 and l_3.

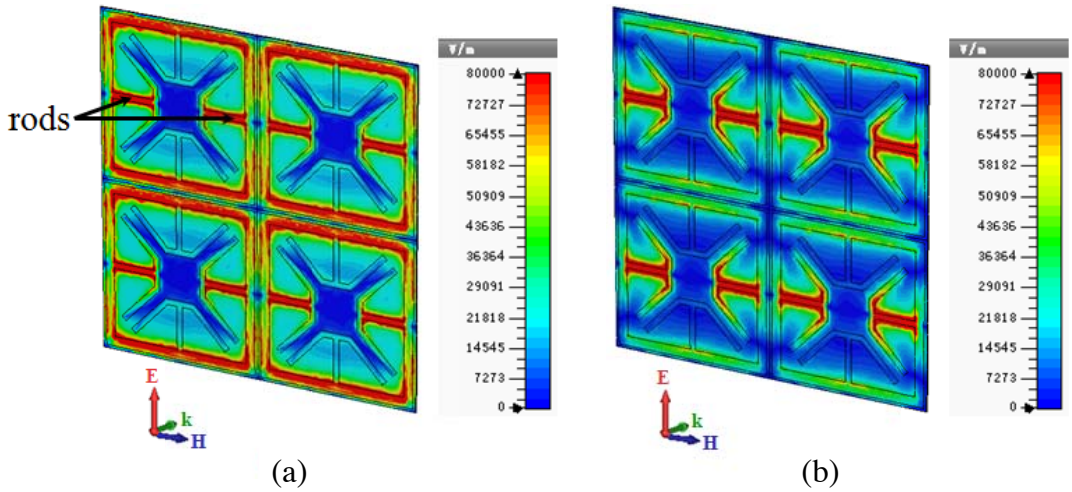

Figure 5. Electric field distributions of proposed FSS for TE polarization under normal incidence: (a) 16.6 GHz; (b) 37 GHz.

be altered with varying the perimeter of square loop. Hence, width g_1 of the square loop becomes the only structural parameters we can change, so that the control of the first passband without affecting the second passband can be achieved. Similarly, the second passband can be modulated with the first passband fixed just by adjusting the geometry of stubs excluding area of rods. The analyses of electric field distribution positively explain the independent controllability of two passbands of the proposed FSS, which have been represented in Figure 4.

3. EXPERIMENT AND MEASUREMENT RESULTS

As shown in Figure 6(a), to further prove the simulation results, a prototype of the proposed FSS with a size of 400 mm × 400 mm is fabricated by using standard printed circuit board photographic and wet-etch techniques. The prototype totally incorporates an array of 166 × 166 elements. An enlarged view of the element is also depicted in the inset. The measurement setup illustrated in Figure 6(b) consists of a plane-wave chamber equally divided by a microwave absorber loaded rotatable screen, thus enabling the

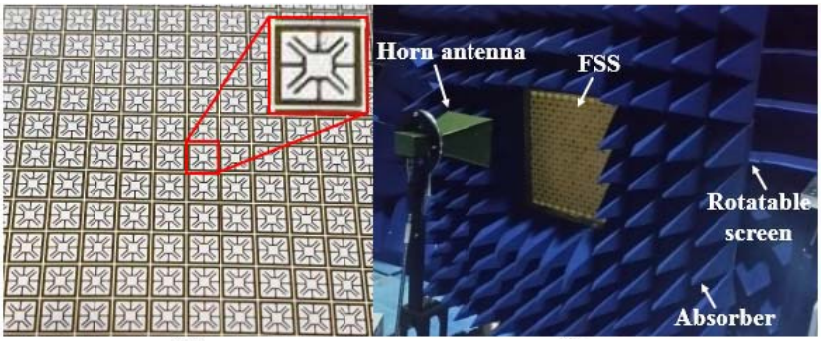

(a) (b)

Figure 6. Photograph of the experiment: (a) fabricated FSS; (b) measurement setup.

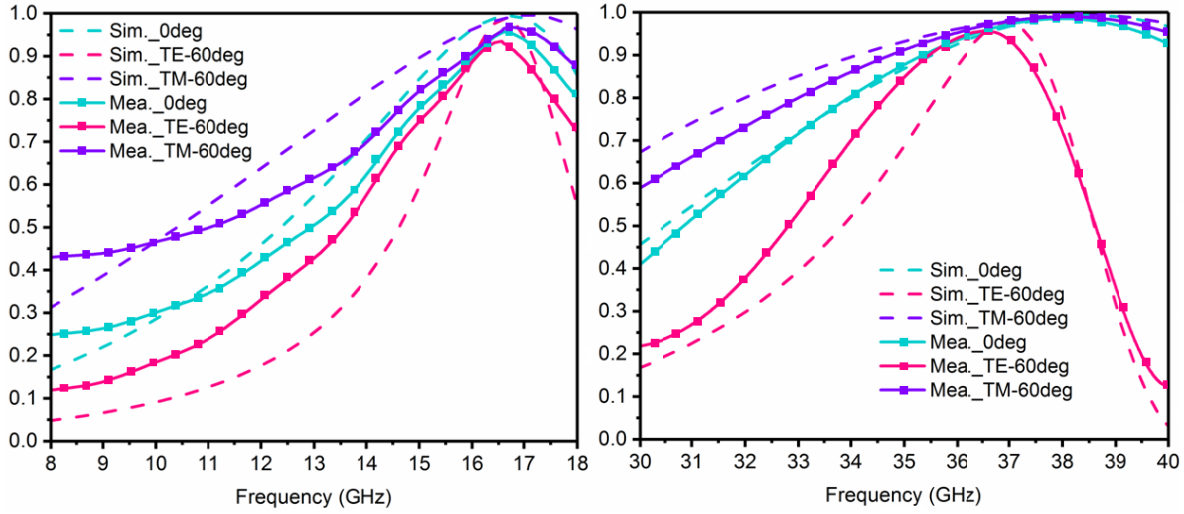

(a) (b)

Figure 7. Comparison between simulated and measured results of the proposed FSS: (a) first pass-band; (b) second pass-band.

transmission measurement under various incident angles to be possible. The rotatable screen is made of aluminum alloy. In the center of screen, a square aperture accepting the FSS prototype under test is placed. A pair of pyramidic horn antennas connected to a vector network analyzer (Agilent N5244A) work as the transmitting and receiving antennas. To accurately control the angles of incidence, the bottom of rotatable screen is connected to an electronic controlled device, while the horn antennas always keep still. The microwave absorber attached to front side of the screen decreases the diffraction of electromagnetic waves, especially at a large incident angle, which can avoid incorrect measurement results. In order to measure the dual-band performance of FSS, two kinds of horn antennas separately operating at $8 \sim 18$ GHz and $26.5 \sim 40$ GHz are utilized in this experiment. The measurement for another polarization can be easily realized by rotating the horn antennas 90°.

Figure 7 represents the simulation and measurement results of the proposed FSS for TE and TM polarizations under various incident angles at the two resonant passbands. It can be observed that the measured results are in a good agreement with the simulated ones except for a frequency shift less than 1.5% for both TE and TM polarizations as the incident angle is up to 60°. The discrepancy between simulation and measurement results is mostly ascribed to the fabrication tolerances and measurement limitation. Anyway, this measurement positively confirm the resonance stability of the proposed FSS at various incident angles for both polarizations.

4. CONCLUSION

A novel dual-band FSS element with a size of $0.133\lambda_0 \times 0.133\lambda_0$ is presented in this paper. The miniaturization design of unit cell definitely results in high resonant stability for different incident angles and polarizations. In addition, the two passbands provided by the FSS can be controlled independently, which means that the FSS structure we proposed has great flexibility to achieve various requirements working in different frequency bands. To further verify the correctness of our design, a prototype of FSS was fabricated and measured. The measurement results show good agreement with the numerical simulation at different incident angles from 0° to 60° for both TE and TM polarizations. With the excellent performance, the designed FSS has a considerable value in the application of multi-functional wireless communication.

REFERENCES

1. Munk, B. A., *Frequency Selective Surfaces: Theory and Design*, Wiley, New York, USA, 2000.
2. Afzal, M. U., A. Lalbakhsh, and K. P. Esselle, "Electromagnetic wave beam-scanning antenna using near-field rotatable graded-dielectric plates," *J. Appl. Phys.*, Vol. 124, 912–915, 2018.
3. Lalbakhsh, A., M. U. Afzal, and K. P. Esselle, "Multiobjective particle swarm optimization to design a time-delay equalizer metasurface for an electromagnetic band-gap resonator antenna," *IEEE Antennas Wireless Propag. Lett.*, Vol. 16, 912–915, 2017.
4. Lalbakhsh, A., M. U. Afzal, K. P. Esselle, and S. L. Smith, "Low-cost non-uniform metallic lattice for rectifying aperture near-field of electromagnetic bandgap resonator antennas," *IEEE Trans. Antennas Prppag.*, Vol. 68, 3328–3335, 2020.
5. Yu, N., P. Genevet, M. A. Kats, F. Aieta, J. P. Tetienne, F. Capasso, and Z. Gaburro, "Light propagation with phase discontinuities: Generalized laws of reflection and refraction," *Science*, Vol. 334, 333–337, 2011.
6. Cui, T. J., M. Q. Qi, X. Wan, J. Zhao, and Q. Cheng, "Coding metamaterials, digital metamaterials and programmable metamaterials," *Light Sci. Appl.*, Vol. 3, e218, 2014.
7. High, A. A., R. C. Devlin, A. Dibos, M. Polking, D. S. Wild, J. Perczel, N. P. Deleon, M. D. Lukin, and H. Park, "Visible-frequency hyperbolic metasurface," *Nature*, Vol. 522, 192, 2015.
8. Phan, T., D. Sell, E. W. Wang, S. Doshay, K. Edee, J. Yang, and J. A. Fan, "High-efficiency, large-area, topology-optimized metasurfaces," *Light Sci. Appl.*, Vol. 8, 48, 2019.
9. Chu, H., Q. Li, B. Liu, J. Luo, S. Sun, Z. H. Hang, L. Zhou, and Y. Lai, "A hybrid invisibility cloak based on integration of transparent metasurfaces and zero-index materials," *Light Sci. Appl.*, Vol. 7, 50, 2018.
10. Fedotov, V. A., J. Wallauer, M. Walther, M. Perino, N. Papasimakis, and N. I. Zheludev, "Wave vector selective metasurfaces and tunnel vision filters," *Light Sci. Appl.*, Vol. 4, e306, 2015.
11. Zabri, S. N., R. Cahill, and A. Schuchinsky, "Compact FSS absorber design using resistively loaded quadruple hexagonal loops for bandwidth enhancement," *Electron. Lett.*, Vol. 51, 162–164, 2015.
12. Akbari, M., S. Gupta, M. Farahani, A. R. Sebak, and T. A. Denidni, "Gain enhancement of circularly-polarized dielectric resonator antenna based on FSS superstrate for MMW applications," *IEEE Trans. Antennas Prppag.*, Vol. 64, 5542–5546, 2016.
13. Bouslama, M., M. Traii, T. A. Denidni, and A. Gharsallah, "Beam-switching antenna with a new reconfigurable frequency selective surface," *IEEE Antennas Wireless Propag. Lett.*, Vol. 15, 1159–1162, 2016.
14. Narayan, S., G. Gulati, B. Sangeetha, and R. U. Nair, "Novel metamaterial element based FSS for airborne radome applications," *IEEE Trans. Antennas Prppag.*, Vol. 66, 4695–4707, 2018.
15. Wang, H., P. Kong, W. Cheng, W. Bao, X. Yu, L. Miao, and J. Jiang, "Broadband tunability of polarization-insensitive absorber based on frequency selective surface," *Sci. Rep.*, Vol. 6, 23081, 2016.

16. Lalbakhsh, A., M. U. Afzal, and K. P. Esselle, "Simulation-driven particle swarm optimization of spatial phase shifters," *International Conference on Electromagnetics in Advanced Applications*, 2016.
17. De Alcantara Neto, M. C., H. R. O. Ferreira, J. P. L. Araújo, F. J. B. Barros, A. G. Neto, M. O. Alencar, and G. P. S. Cavalcante, "Compact ultra-wideband FSS optimised through fast and accurate hybrid bio-inspired multiobjective technique," *IET Microwaves, Antennas & Propagation*, Vol. 14, 884–890, 2020.
18. Lalbakhsh, A., M. U. Afzal, K. P. Esselle, and S. Smith, "Design of an artificial magnetic conductor surface using an evolutionary algorithm," *Proc. 19th IEEE International Conference on Electromagnetics in Advanced Applications*, 2017.
19. Hu, X.-D., X.-L. Zhou, L.-S. Wu, L. Zhou, and W.-Y. Yin, "A miniaturized dual-band frequency selective surface (FSS) with closed loop and its complementary pattern," *IEEE Antennas Wireless Propag. Lett.*, Vol. 8, 1374–1377, 2009.
20. Zanganeh, E., M. Fallah, A. Abdolali, and N. Komjani, "New approach to design dual-band frequency selective surface based on frequency response tunning of each individual layer," *Microw. Opt. Technol. Lett.*, Vol. 58, 1423–1429, 2016.
21. Campos, A. L. P. S., R. H. C. Manicoba, L. M. Araujo, and A. G. D'Assuncao, "Analysis of simple FSS cascading with dual band response," *IEEE Trans. Magnetics*, Vol. 46, 3345–3348, 2010.
22. Salehi, M. and N. Behdad, "A second-order dual X-/Ka-band frequency selective surface," *IEEE Microw. Wireless Compon. Lett.*, Vol. 18, 785–787, 2008.
23. Ray, A., M. Kahar, S. Biswas, D. Sarkar, and P. P. Sarkar, "Dual tuned complementary structure frequency selective surface WLAN applications," *J. Microw. Optoelectron. Electromagn. Appl.*, Vol. 11, 144–152, 2012.
24. Li, M. and N. Behdad, "A third-order bandpass frequency selective surface with a tunable transmission null," *IEEE Trans. Antennas Propag.*, Vol. 60, 2109–2113, 2012.
25. Romeu, J. and R.-S. Yahya, "Fractal FSS: A novel dual-band frequency selective surface," *IEEE Trans. Antennas Propag.*, Vol. 48, 1097–1105, 2000.
26. Romeu, J. and Y. Rahmat-Samii, "Dual band FSS with fractal elements," *Electron. Lett.*, Vol. 35, 702–703, 1999.
27. Silva, P. H. da F., A. F. dos Santos, R. M. S. Cruz, and A. G. D'Assunção, "Dual-band bandstop frequency selective surfaces with gosperprefractal elements," *Microw. Opt. Technol. Lett.*, Vol. 54, 771–775, 2012.
28. De Lucena Nóbrega, C., M. R. da Silva, P. H. da Fonseca Silva, and A. G. D'Assunção, "Analysis and design of frequency selective surfaces using teragon patch elements for WLAN applications," *Journal of Electromagnetic Waves and Applications*, Vol. 28, No. 11, 1282–1292, 2014.
29. Li, B. and Z. Shen, "Dual-band bandpass frequency selective structures with arbitrary band ratios," *IEEE Trans. Antennas Propag.*, Vol. 62, 5504–5512, 2014.